Secondary Structure and Zinc Ligation of Human Recombinant Short-Form Stromelysin by Multidimensional Heteronuclear NMR

Paul R. Gooley,*,‡ Bruce A. Johnson,‡ Alice I. Marcy,‡ Gregory C. Cuca,‡ Scott P. Salowe,‡ William K. Hagmann,§ Craig K. Esser,§ and James P. Springer‡

Departments of Biophysical Chemistry and Medicinal Chemical Research, Merck Research Laboratories, P.O. Box 2000, Rahway, New Jersey 07065

Received May 25, 1993; Revised Manuscript Received July 8, 1993®

ABSTRACT: Stromelysin-1, a member of the matrix metalloendoprotease family, is a zinc protease involved in the degradation of connective tissue in the extracellular matrix. As a step toward determining the structure of this protein, multidimensional heteronuclear NMR experiments have been applied to an inhibited truncated form of human stromelysin-1. Extensive ^{1}H, ^{13}C, and ^{15}N sequential assignments have been obtained with a combination of three- and four-dimensional experiments. On the basis of sequential and short-range NOEs and $^{13}C^{\alpha}$ chemical shifts, two helices have been delineated, spanning residues Asp-111 to Val-127 and Leu-195 to Ser-206. A third helix spanning residues Asp-238 to Gly-247 is characterized by sequential NOEs and $^{13}C^{\alpha}$ chemical shifts, but not short-range NOEs. The lack of the latter NOEs suggests that this helix is either distorted or mobile. Similarly, sequential and interstrand NOEs and $^{13}C^{\alpha}$ chemical shifts characterize a four-stranded β-sheet with three parallel strands (Arg-100 to Ile-101, Ile-142 to Ala-147, Asp-177 to Asp-181) and one antiparallel strand (Ala-165 to Tyr-168). Two zinc sites have been identifed in stromelysin [Salowe et al. (1992) *Biochemistry 31*, 4535–4540]. The NMR spectral properties, including chemical shift, pH dependence, and proton coupling of the imidazole nitrogens of six histidine residues (151, 166, 179, 201, 205, and 211), invariant in the matrix metalloendoprotease family, suggest that these residues are zinc ligands. NOE data indicate that these histidines form two clusters: one ligates the catalytic zinc (His-201, -205, and -211), and the other ligates a structural zinc (His-151, -166, and -179). Heteronuclear multiple quantum correlated spectra and specific labeling experiments indicate His-151, -179, -201, -205, and -211 are in the $N^{\delta 1}H$ tautomer and His-166 is in the $N^{\epsilon 2}H$ tautomer.

The matrix metalloendoproteases (MMP)[1] are a family of enzymes that degrade the protein components of the connective tissue, such as collagen and proteoglycans. These proteases, on the basis of substrate specificity, are divided into three groups: the collagenases digest the interstitial collagens, the gelatinases degrade denatured collagens, and the stromelysins show broad substrate specificity (Murphy et al., 1991). Other characteristics of the MMP family are as follows: expression as zymogens which are activated *in vitro* by organomercurials with the loss of a propeptide piece of approximately 10 kDa; a catalytic mechanism that is dependent on zinc; and activity that is inhibited by tissue inhibitors of metalloprotease (TIMP) (Woessner, 1991). The degradative diseases rheumatoid arthritis and osteoarthritis may result from pathological proteolysis of the cartilage by these enzymes. Although the relative importance of each protease is yet to be determined, stromelysin-1 is believed to play a major role in these diseases, because of its ability to degrade most of the components of the cartilage and its secretion from synoviocytes and chrondocytes is induced by the inflammatory mediator interleukin-1 (Woessner, 1991; Murphy et al., 1986; Saus et al., 1988; MacNaul et al., 1991). Thus, determining the structure of this enzyme may aid the design of potent inhibitors and result in a treatment of arthritis.

Mature stromelysin is a 45-kDa protein; however, the 19-kDa N-terminal catalytic domain (sfSTR) has similar kinetic, catalytic, and inhibitory properties to full-length stromelysin (Marcy et al., 1991). The size of sfSTR and the ability to recover recombinant protein from *Escherichia coli* are attractive for structural studies by NMR and X-ray crystallography. Structures have been determined for several metallendoproteases, including thermolysin (Mathews et al., 1972) and astacin (Bode et al., 1992; Gömis-Ruth et al., 1993). In these proteins a single catalytic zinc has been observed. Surprisingly, metal analysis of sfSTR showed the presence of two zincs per protein molecule (Salowe et al., 1992). EXAFS spectroscopy suggests that the two zinc sites of sfSTR are independent and that each metal is ligated by four nitrogen or oxygen moieties (Holz et al., 1992). Treatment of sfSTR with *o*-phenanthroline removes only 1 equiv of zinc and results in the loss of peptidase activity. Addition of either zinc or cobalt restores activity, suggesting that the exchangeable zinc plays a catalytic role whereas the nonexchangeable zinc is structural (Salowe et al., 1992). The presence of an apparent structural zinc, in addition to the catalytic metal, suggests that members of the MMP family comprise a unique class of metallendoproteases. This report provides the first structural data for a member of this family of enzymes and presents further evidence for the presence of two zincs in stromelysin.

* Address correspondence to this author at Merck Research Laboratories, Department of Biophysical Chemistry, RY80Y-103, P.O. Box 2000, Rahway, NJ 07065.

‡ Department of Biophysical Chemistry.

§ Department of Medicinal Chemistry Research.

® Abstract published in *Advance ACS Abstracts*, November 1, 1993.

[1] Abbreviations: MMP, matrix metalloendoproteases; NMR, nuclear magnetic resonance; EXAFS, extended X-ray absorption fine structure; HMQC, heteronuclear multiple quantum correlated; HSQC, heteronuclear single quantum correlated; COSY, correlated spectroscopy; NOE, nuclear Overhauser effect; NOESY, NOE spectroscopy; TOCSY, total correlated spectroscopy; sfSTR, stromelysin-1 (EC 3.4.24.17) truncated at residue 255; TSP, (trimethylsilyl-2,2,3,3-$^{2}H_4$)propionate; 2D, two-dimensional; 3D, three-dimensional; 4D, four-dimensional.

0006-2960/93/0432-13098$04.00/0 © 1993 American Chemical Society

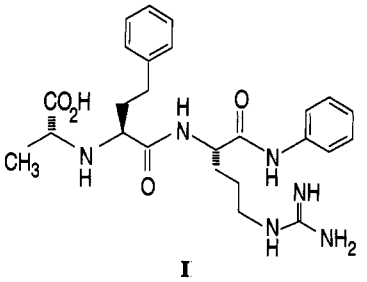

I

FIGURE 1: Carboxyalkyl inhibitor (I) of sfSTR, *N*-[(*R*)-carboxyethyl]-α-(*S*)-(2-phenylethyl)glycyl-L-arginine-*N*-phenylamide (Chapman et al., unpublished).

MATERIALS AND METHODS

Sample Preparation. Recombinant BL21(DE3) *E. coli* containing the plasmid specifying truncated pro-sfSTR were grown in M9 minimal media (Maniatis et al., 1982) containing 100 mg/L ampicillin (Sigma, St. Louis, MO) and either 0.4% glucose, 1 g/L $^{15}NH_4Cl$ (99% ^{15}N) (Isotec, Miamisburg, OH; Cambridge, Woburn, MA; Merck Isotopes, Canada), and 0.1 g/L ^{15}N-algal hydrolysate (99% ^{15}N) (Martek, Columbia, MD; Merck Isotopes, Canada) or 0.2% [$^{13}C_6$]glucose (99% ^{13}C) (Isotec, Miamisburg, OH; Cambridge, Woburn, MA; Merck Isotopes, Canada) 1 g/L $^{15}NH_4Cl$, and 0.1 g/L ^{13}C/^{15}N-algal hydrolysate. To obtain ^{15}N protein specifically labeled at the $N^{\delta 1}$ position in histidine, recombinant *E. coli* were grown in the above media with 0.4% glucose, amino acids (except histidine), and nucleosides (LeMaster & Richards, 1985). At induction, 30–50 mg/L of [$^{15}N^{\delta 1}$]His (99% ^{15}N) (Cambridge, Woburn, MA) was added.

Purification of pro-sfSTR and activation to sfSTR has been previously described (Marcy et al., 1991). Samples were prepared by repeated dilution with 50 mM acetate-d_3 (at pH 5.5) or 10 mM MES (at pH 6.5), 5 mM $CaCl_2$, 0.02% NaN_3, and 10% or 100% ^2H_2O at 4 °C and concentration using a Centricon-3 (Amicon, Danvers, MA). At the final concentration, samples of sfSTR were inhibited with 10% molar excess of I (Figure 1). To prevent autoactivation, 1% molar of I was added to samples of pro-sfSTR. One-dimensional ^{15}N and 2D ^1H, ^{15}N HSQC spectra were collected between 10 and 40 °C, with samples typically 0.4–1 mM. All 3D and 4D experiments were acquired at 40 °C with 0.4 mM protein. In preparation for ^1H–^2H exchange experiments, samples of inhibited sfSTR were exchanged three times in the above buffer with 100% ^2H_2O at 4 °C overnight and were heated at 40 °C for 30 min before acquiring a 2D ^1H, ^{15}N HSQC spectrum. An additional spectrum was acquired after ^1H–^2H exchange for 3 days at 40 °C.

NMR Spectroscopy. Unless noted, all spectra were acquired on a 500-MHz Varian Unity equipped with three RF channels. One-dimensional ^{15}N spectra were acquired with 40 000- or 10 000-Hz sweep widths, 60° pulse width, 1-s recycle time, and 80 000 transients. One-dimensional ^{15}N spectra of inhibited sfSTR or pro-sfSTR, selectively enriched with [$^{15}N^{\delta 1}$]-His, were acquired at 600 MHz with a 12 500-Hz sweep width and 60 000 or 200 000 transients, respectively.

Four-dimensional HCa(CO)NNH and HCaNNH spectra (Boucher et al., 1992a,b; B. A. Johnson, unpublished) were acquired with constant-time evolution (Powers et al., 1991) during t_2 and t_3 and composite pulse ^1H decoupling during ^{13}C evolution to minimize the relaxation effects of ^{13}C antiphase magnetization (Bax et al., 1990c; Norwood et al., 1990). Both 4D experiments were acquired with sweep widths of 1800 Hz (^1H, t_1), 1600 Hz (^{13}C, t_2), 1100 Hz (^{15}N, t_3), and 7300 Hz (^1H, t_4) and 8 transients for each FID. The acquired matrix was 32 × 8 × 8 × 512 complex points. The t_2 (^{13}C) and t_3 (^{15}N) dimensions were extended to 16 complex data points by linear prediction (Barkhuijsen et al., 1985; B. A. Johnson, unpublished). All dimensions were multiplied by 90° sine bell window functions and, after zero filling, Fourier transformed to a final matrix of 64 × 32 × 32 × 512 real data points.

Three-dimensional HCCH COSY (Bax et al., 1990a) and TOCSY (Bax et al., 1990b), 3D ^{13}C NOESY-HMQC (Ikura et al., 1990), and 3D ^{15}N NOESY-HMQC (Zuiderweg & Fesik, 1989; Messerle et al., 1989) data were acquired with standard pulse sequences, and 16 transients for each FID. The first two experiments were acquired with 3400 Hz (t_1), 3200 Hz (t_2), and 4000 Hz (t_3) sweep widths. The 3D ^{13}C NOESY-HMQC experiment was acquired with 6000 Hz (t_1), 7900 Hz (t_2), and 6000 Hz (t_3). The sweep widths for the 3D ^{15}N NOESY-HMQC were 6200 Hz (t_1), 1100 Hz (t_2), and 8400 Hz (t_3). The acquired matrices were 128 × 32 × 512 complex for the ^{13}C spectra and 110 × 32 × 1024 complex for the ^{15}N spectra, and the final Fourier-transformed matrices were 256 × 64 × 512 real data points.

Two-dimensional ^1H, ^{15}N HSQC spectra (Bodenhausen & Ruben, 1980; Messerle et al., 1989) were acquired with 10 000-Hz, 1024 complex data points (t_2) and 10 000- or 1600-Hz, 64–256 complex data points (t_1). A 2D ^1H, ^{15}N HMQC spectrum (Summers et al., 1986) was acquired at 600 MHz with 7200-Hz, 512 complex data points (t_2) and 7500-Hz, 64 complex data points (t_1). This latter experiment was acquired on a sample of inhibited sfSTR in buffer prepared with ^2H_2O, and the delay where ^1H and ^{15}N magnetization become antiphase was set to 22 ms, thus minimizing $^1J_{NH}$ couplings of 90–95 Hz (Pelton et al., 1993).

Spectra were processed using a modified version of FELIX (Biosym, Inc.). For spectra acquired in ^1H_2O, the residual water signal and artifacts arising from this signal were effectively removed by a postacquisition method (Johnson, 1992). Chemical shifts for ^1H were referenced to residual HDO, which resonates at 4.64 ppm relative to TSP at 40 °C. The corresponding references of 4.64 ppm for the ^{13}C and ^{15}N dimensions were obtained by multiplying the ^1H spectrometer frequency by 0.251 449 54 and 0.101 329 144 4, respectively (Bax & Subramanian, 1986; Live et al., 1984). For experiments in ^1H_2O where only NH protons are detected, the upfield half of the spectrum was discarded. Spectra were displayed and analyzed by a software package, NMRView, that has been developed in our laboratories (B. A. Johnson and R. Blevins, unpublished).

RESULTS AND DISCUSSION

Sequential Assignment of Stromelysin-1. Briefly, sequential assignment of neighboring residues was accomplished by a combination of 4D HCaNNH and HCa(CO)NNH, 3D HCCH COSY and TOCSY, and 3D ^{15}N NOESY-HMQC. The two 4D experiments can rapidly establish sequential *J* connectivities, as many single planes contain only one peak (Figure 2). Further, Pro and Gly serve as "stop" residues in this procedure because Pro will not show an interresidue connectivity to an $i - 1$ residue and Gly will not show an interresidue connectivity to an $i + 1$ residue, and neither will have an intraresidue connectivity (Campbell-Burk et al., 1992). Therefore, strips of a unique number of sequentially assigned backbone resonances, terminated by either Gly or Pro, may be specifically located in the primary sequence. Although a number of strips were rapidly identified by this method, multiple sequential connectivity pathways are possible whenever more than one peak exists in a plane, a situation that requires some knowledge of the side chain of the residue

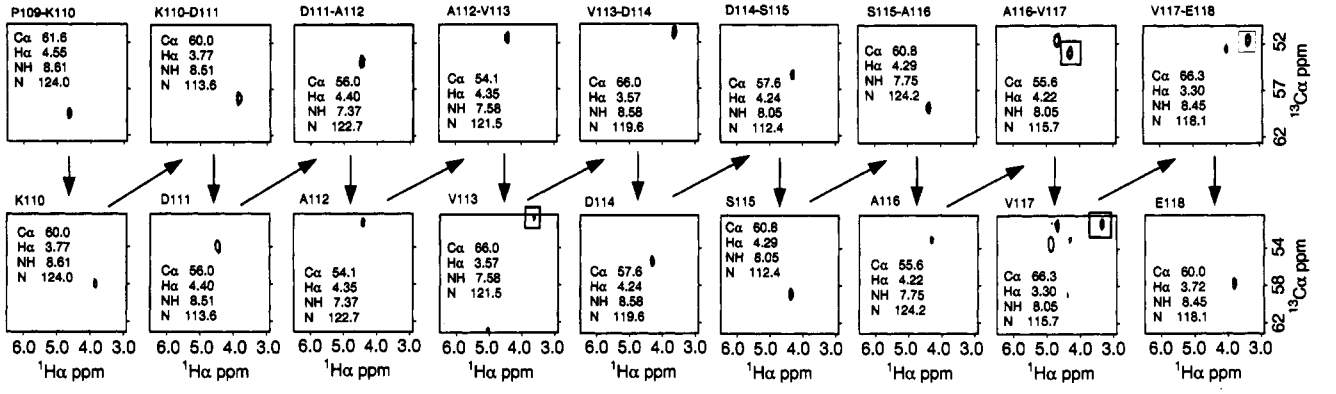

FIGURE 2: Sequential assignment of backbone nuclei by J correlations of sfSTR. Sample conditions were 0.4 mM inhibited ^{15}N, ^{13}C sfSTR in 50 mM acetate-d_3, pH 5.5, 5 mM $CaCl_2$, and 0.01% NaN_3 and 40 °C. Each peak within a plane corresponds to four frequencies ($^1H^\alpha$, $^{13}C^\alpha$, ^{15}N, and NH). Sequential residues are connected by first locating a peak in a plane of either of the 4D HCaNNH or 4D HCa(CO)NNH and then finding a corresponding peak in the alternate experiment with the same pair of nuclei, either $^{13}C^\alpha H^\alpha$ or ^{15}NH. The sequential connectivities are shown for the segment Pro-109 to Glu-118 (using the sequence numbering of pro-sfSTR), a part of a helix, starting with the interresidue correlation between the $^{13}C^\alpha H^\alpha$ of Pro-109 and the ^{15}NH of Lys-110. Where there is more than one peak in a plane, the correct correlation is boxed; however, the centers of the additional peaks in this figure are not in the planes shown, and thus assignment is unambiguous.

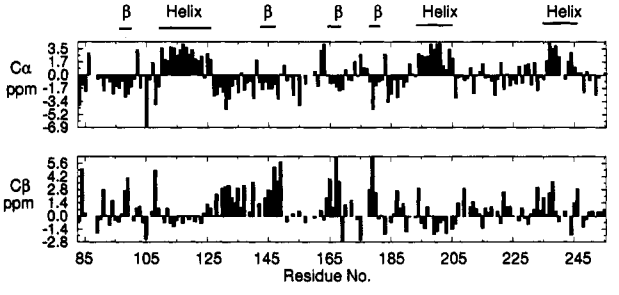

FIGURE 3: Deviation from random coil ^{13}C chemical shift for C^α and C^β assigned resonances. Residues are numbered according to the sequence of pro-sfSTR. Chemical shifts are plotted as observed less random coil (Spera & Bax, 1991). The random coil chemical shifts for His, which are not included in this reference, were taken from Richarz and Wüthrich (1978). Regions of helix and β-strand are indicated.

identified in the sequential assignment. This latter information is obtained from the above 3D HCCH experiments where, using the $^{13}C^\alpha H$ resonances assigned in the 4D experiments, slices were analyzed to obtain assignments of the side chain resonances. Verification of sequential assignment and extension of these assignments were obtained by observing the sequential NOEs (d_{NN}, $d_{\alpha N}$, $d_{\beta N}$) in the 3D ^{15}N NOESY-HMQC experiment, which was guided in part by the ^{15}NH resonance assignments obtained in the 4D experiments, and further by comparison of the observed $^{13}C^\alpha$ and $^{13}C^\beta$ chemical shift to those for small peptides (Figure 3) (Spera & Bax, 1991). Thus, where this chemical shift difference is positive for the C^α and negative for C^β, the expected principal NOE is d_{NN}, whereas if the difference is negative for the C^α and usually positive for C^β, the expected principal NOE is $d_{\alpha N}$.

With the above protocol, approximately 80% of the resonances were readily assigned. After completion of the sequential assignments by the 4D experiments, all assigned ^{15}NH resonances were located in 2D ^{1}H, ^{15}N HSQC spectra. Using the chemical shifts of the remaining unassigned ^{15}NH resonances, several additional sequential assignments were identified in the 3D ^{15}N NOESY-HMQC, particularly for Leu-207 to Gly-208 and His-211 to Ala-213, which showed no identifiable correlations in the 4D HCaNNH and HCa(CO)NNH experiments. Assignment of the various aromatic spin systems was obtained in 3D HCCH TOCSY, where the carrier frequency for ^{13}C was positioned in the middle of this region (124.5 ppm), and a number of these systems were specifically assigned by NOEs between ring protons and backbone atoms in 3D ^{13}C NOESY-HMQC spectra. This

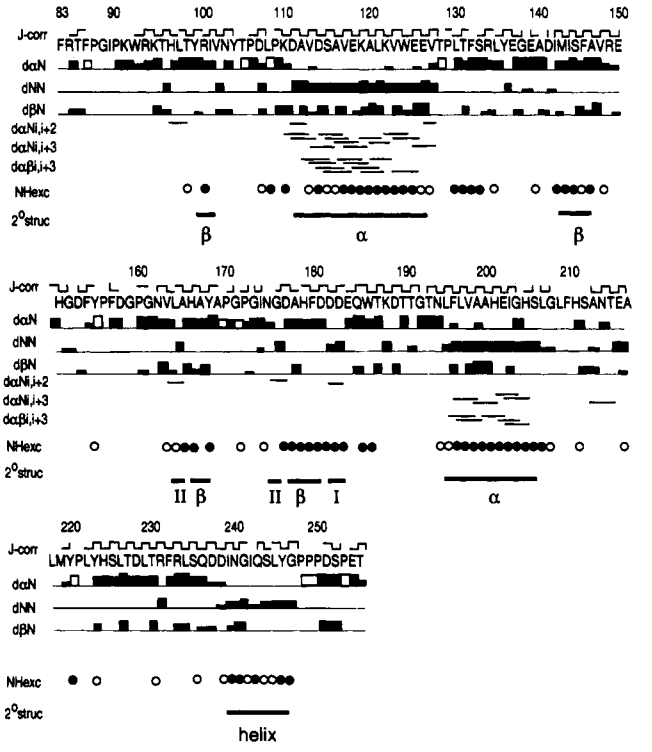

FIGURE 4: Summary of sequential assignments by J correlations, sequential NOEs, short-range NOEs, ^{1}H–^{2}H exchange experiments for NH protons, and secondary structure of inhibited sfSTR. Residues are numbered according to the sequence of pro-sfSTR. The J correlation data summarize the sequential of the 4D HCaNNH and HCa(CO)NNH experiments, where an interresidue correlation is indicated by (–) and an intraresidue correlation by (|). The intensity of the sequential NOE is proportional to the thickness of the bar. Sequential NOEs, $C^\alpha H(i)$ to $C^\delta H(i+1)$ for Xxx-Pro are shown by unfilled bars. NH protons that exchange for ^{2}H within 3 days are shown by O, whereas protons that are still present are shown by ●. Secondary structural elements are defined by the NOE data (Wüthrich, 1986). Type I and II turns are indicated where sequential and short-range NOEs and a slowly exchanging NH proton in position $i + 3$ are observed. The strands of a β-sheet are delineated by interstrand NOEs (Figure 6C).

procedure was successful for the majority of His, Tyr, and Trp residues, but only 4 of the 10 Phe ring systems have been partially assigned. The assignment of the His residues is discussed in detail below. By appropriate selection of the delays in the 4D HCaNNH spectrum (Kay et al., 1991), 10 of the 13 Gly spin systems have been successfully assigned. Resonance overlap has prevented the complete assignment of

Table I: ^{1}H, ^{13}C, ^{15}N Chemical Shift Assignments for Inhibited sfSTR at pH 5.5 and 40 °C[a]

Ala, residue no.	N	HN	C^{α}	H^{α}	C^{β}	H^{β}	Ala, residue no.	N	HN	C^{α}	H^{α}	C^{β}	H^{β}
112	122.67	7.37	54.09	4.35	19.81	1.63	169	121.46	7.62	50.44	4.18	16.23	0.25
116	124.25	7.75	55.60	4.22	19.02	1.53	178	117.93	8.12	51.48	4.93	21.80	1.06
120	123.14	8.02	55.60	4.02	19.48	1.40	199	121.42	9.25	55.61	4.06	17.03	1.16
140	131.39	8.03	49.25	4.52	22.60	0.95	200	120.06	8.77	56.41	3.88	17.42	0.99
147	125.43	9.32	51.11	4.91	24.19	1.08	213	127.05	8.48	52.23	4.67	19.81	1.51
165	115.64	7.77	51.23	4.58	22.99	1.31	217	123.85	7.84	52.03	4.63	19.41	1.86
167	122.77	8.73	50.74	5.08	25.38	1.49							

Arg, residue no.	N	HN	C^{α}	H^{α}	C^{β}	H^{β}	C^{γ}	H^{γ}	C^{δ}	H^{δ}	Arg, residue no.	N	HN	C^{α}	H^{α}	C^{β}	H^{β}	C^{γ}	H^{γ}	C^{δ}	H^{δ}
84	?	?	54.83	4.82	35.32	1.82, 2.07	28.96	1.85	44.08	3.40	149	117.81	9.60	56.23	3.86	28.86[b]	2.01	27.40	1.66	42.48	3.30
93	123.28	9.26	55.21	4.62	29.36	1.84, 2.22	28.16	1.73, 1.86	43.28	3.29	231	119.80	7.50	54.84	4.45	30.55	2.08, 1.70	27.77[b]	1.56, 1.67	43.68	3.19
100	122.77	8.14	54.56	4.36	?	?	?	?	43.28	3.25	233	126.61	7.02	54.09	4.03	33.34	1.73, 1.52	26.18[b]	1.54, 1.46	43.68	3.15
134	125.97	8.54	55.61	3.58	31.74	1.52, 1.24	27.36	0.51	43.68	2.88, 2.97											

Asn[c] residue no.	N	HN	C^{α}	H^{α}	C^{β}	H^{β}	N^{δ}	H^{δ}	Asn,[c] residue no.	N	HN	C^{α}	H^{α}	C^{β}	H^{β}	N^{δ}	H^{δ}
103	115.92	7.71	51.11	4.75	38.90	3.16, 3.02	111.43	7.46, 7.62	194	127.17	8.27	55.61	4.90	40.98	2.80, 2.97	109.99	7.07, 6.27
162	118.03	9.15	56.01	4.14	38.51	3.15, 2.95	115.32	7.88, 6.87	214	120.36	8.73	53.22	4.72	38.11	2.72, 3.02	112.62	7.74, 6.92
175	118.38	7.23	55.51	4.26	35.42[b]	2.83, 2.28	?	?	240	118.67	9.15	55.21	4.35	37.31	3.09, 2.87	110.57	7.72, 7.04

Asp, residue no.	N	HN	C^{α}	H^{α}	C^{β}	H^{β}	Asp, residue no.	N	HN	C^{α}	H^{α}	C^{β}	H^{β}
107	121.75	8.93	55.57	4.14	41.29	2.75, 3.29	182	128.70	9.90	53.35	5.59	40.89	2.94, 2.54
111	113.64	8.51	56.01	4.40	40.10	2.72, 2.66	183	124.12	9.35	54.47	5.03	37.37	2.70, 2.24
114	119.60	8.58	57.60	4.24	39.70	2.85, 2.69	189	120.91	7.61	52.43	4.96	42.09	2.80, 3.42
141	122.04	8.33	55.91	4.33	?	?	228	119.97	7.75	52.98	4.80	41.69	2.66, 2.83
153	117.22	6.97	51.36	4.58	41.05[b]	3.21, 2.76	237	117.92	8.17	58.35	4.58	43.28	2.88, 2.58
158	116.25	8.02	?	?	?	?	238	116.56	7.41	57.50	4.74	44.47	3.10, 2.89
177	121.17	7.89	54.84	4.70	?	?	251	120.07	8.27	54.02	4.59	41.29	2.66, 2.71
181	123.56	8.22	53.16	4.42	40.50	3.16, 0.74							

Gln,[c] residue no.	N	HN	C^{α}	H^{α}	C^{β}	H^{β}	C^{γ}	H^{γ}	N^{ϵ}	H^{ϵ}
185	126.36	8.36	53.62	4.44	27.77	2.00, 1.77	35.32	2.18, 2.25	112.23	7.42, 6.77
236	122.44	9.06	58.00	3.96	28.56	2.26, 2.11	33.61[b]	2.49	113.57	6.89, 7.46
243	122.48	8.60	57.89	4.24	?	?	34.49	3.02, 2.83	?	?

Glu, residue no.	N	HN	C^{α}	H^{α}	C^{β}	H^{β}	C^{γ}	H^{γ}	Glu, residue no.	N	HN	C^{α}	H^{α}	C^{β}	H^{β}	C^{γ}	H^{γ}
118	118.06	8.45	59.99	3.72	29.76	2.22, 2.07	36.92	2.26, 2.51	150	128.88	8.36	57.67	4.30	?		?	?
125	122.23	8.59	59.19	4.00	30.95	2.38	36.52	2.87, 2.52	184	115.91	7.31	52.92	4.58	?		?	?
126	111.88	7.90	58.40	4.19	30.55	2.24, 2.09	36.92	2.64, 2.43	202	115.96	8.86	57.60	4.36	29.36	2.21	?	2.43, 2.30
137	116.79	7.53	54.42	4.41	32.94	1.94, 2.14	?	?	216	119.56	8.77	56.01	4.39	30.55	2.15, 2.00	?	2.34
139	119.44	8.17	55.61	4.39	30.15	1.93, 1.87	?	2.18	254	121.36	8.41	56.41	4.39	30.15	2.13, 1.98	36.52	2.33, 2.22

Gly, residue no.	N	HN	C^{α}	H^{α}	Gly, residue no.	N	HN	C^{α}	H^{α}
138	108.52	8.46	44.08	4.10, 3.81	192	111.93	7.43	45.27	4.26, 3.62
152	109.14	8.43	44.87	4.11, 3.64	204	109.02	7.44	48.45	3.83, 2.46
161	119.31	11.38	43.63	4.15, 3.60	208	108.54	8.49	44.87	4.90, 3.49
171	107.87	5.54	44.48	4.03	241	108.98	8.14	?	?
173	109.82	8.74	46.82	3.90	247	109.06	8.37	43.94	3.99
176	118.66	7.69	46.06	4.57, 4.14					

His, residue no.	N	HN	C^{α}	H^{α}	C^{β}	H^{β}	$C^{\delta 2}$	$H^{\delta 2}$	$C^{\epsilon 1}$	$H^{\epsilon 1}$	$N^{\delta 1}$	$H^{\delta 1}$	$N^{\epsilon 2}$	$H^{\epsilon 2}$
96[d]	119.56	7.14	53.35	5.13	28.96	3.10, 2.90	?	?	?	?	?	?	?	?
151	121.41	9.14	54.31	5.13	28.96	3.42, 2.74	125.89	6.34	137.84	7.12	171.38	11.76[e]	203.96	
166	110.54	9.09	54.03	4.85	30.50[b]	3.42, 3.01	?	7.35	138.55	8.21	206.73		170.94	13.55[e]
179	120.54	9.10	50.54	5.77	35.86[b]	2.67, 3.13	122.76	6.58	139.52	8.78	178.20	12.77[e]	199.44	
201	117.13	7.69	59.20	3.98	28.87[b]	2.38, 2.89	125.74	6.51	135.53	7.78	178.10	12.4[e]	206.22	
205	119.56	7.07	57.27	5.49	28.16	2.86, 4.08	126.73	7.55	135.58	6.47	169.32		210.73	
211	?	?	56.03	5.20	30.51[b]	2.83, 2.34	124.76	7.22	139.50	8.49	176.33		201.91	
224[d]	121.25	5.89	53.72	4.42	30.55	3.12, 3.05	?	?	?	?	?	?	?	?

Ile, residue no.	N	HN	C^{α}	H^{α}	C^{β}	H^{β}	C^{γ}	$H^{\gamma 1}$	C^{δ}	H^{δ}	C^{γ}	$H^{\gamma 2}$
89	?	?	60.78	3.91	36.19	2.11	27.77	1.08, 1.44	13.84	0.91	20.61	0.93
101	128.37	8.37	60.78	4.39	37.49	1.72	27.37	1.66	14.24	1.03	17.82	0.35
142	123.51	8.59	60.38	4.28	39.30	1.88	25.26	1.36, 1.52	15.04	0.80	15.44	0.99
144	127.81	9.15	60.40	5.49	39.92	1.97	29.36	1.04, 1.76	15.04	0.81	17.42	0.75
174	131.87	8.90	61.17	4.25	37.69	1.59	28.96	1.12	15.04	0.70	16.63	0.41
203	118.31	8.93	61.98	3.87	36.19	2.00	29.76	1.35, 1.30	11.46	0.57	18.62	0.62
239	119.93	7.93	65.16	3.63	38.51	1.78	30.55	1.84	13.45	0.80	17.42	0.91
242	125.17	8.73	60.78	4.37	38.51	2.22	30.55	1.72, 1.94	15.83	0.94	21.40	1.58

Table I (Continued)

Leu, residue no.	N	HN	C^α	H^α	C^β	H^β	C^γ	H^γ	C^δ	H^δ
97	127.47	8.25	52.90	4.54	45.27	0.97, 1.29	28.16	0.81	25.38, 23.39	−0.02, −0.22
108	116.17	7.03	51.24	4.94	?	?	26.57	1.58	24.98, 26.97	1.02, 0.62
121	114.78	7.67	57.20	3.73	41.68[b]	0.61, 1.46	25.78	1.19	25.38, 22.20	−0.51, −0.42
130	117.79	7.34	54.31	4.52	?	?	27.77	1.19	26.57, 22.20	0.40, 0.30
135	125.54	8.60	52.83	4.72	45.27	1.69, 1.28	27.77	1.57	25.39, 23.39	0.85, 0.95
164	129.78	9.59	55.01	4.64	44.23[b]	1.70, 1.73	27.37	2.01	26.18, 21.80	0.20, 0.47
195	129.06	8.10	57.64	4.58	41.58	1.59, 1.88	27.77	1.19	22.20, 28.96	−0.15, 0.73
197	119.59	8.72	57.57	3.25	43.28	1.77	27.37	1.82	25.38, 25.38	0.88, 0.70
207	113.95	7.68	54.42	4.59	?	?	26.18	1.97	25.78, 22.60	0.34, 0.79
209	120.48	8.67	54.42	4.74	45.28[b]	1.70	26.97	1.48	26.97, 22.60	0.99, 0.74
218	?	?	54.38	4.59	43.28	1.52, 1.65	?	?	24.19, 25.84	1.00, 1.05
222	118.19	6.59	53.22	5.03	44.87	1.67	28.16	1.53	25.38, 24.58	1.05, 0.96
226	123.98	7.69	53.97	4.57	?	?	28.16	1.72	22.99, 28.16	1.32, 0.87
229	125.72	8.85	56.41	4.18	42.09	1.77, 1.66	?	?	25.78, 24.64	1.02, 0.97
234	122.02	8.40	54.82	3.93	42.88	1.51	27.37	1.46	26.97, 24.19	0.37, 0.25
245	120.10	6.73	56.15	4.14	43.68	1.78, 0.33	26.97	1.58	26.18, 24.19	0.91, 0.79

Lys, residue no.	N	HN	C^α	H^α	C^β	H^β	C^γ	H^γ	C^δ	H^δ	C^ϵ	H^ϵ
91	113.98	7.34	54.42	4.49	35.32	1.87, 1.75	23.39	1.50, 1.16	30.55	1.57, 1.47	41.69	2.93
94	116.61	7.56	54.02	4.81	34.13	2.01, 1.96	23.79	1.41, 1.26	30.55	1.79	42.09	3.00
110	124.01	8.61	59.99	3.77	32.54	1.51, 1.40	24.98	1.06, 0.72	29.36	1.32, 1.23	41.69	2.75, 2.79
119	119.30	8.31	59.19	3.98	32.14	1.76, 1.91	26.18	1.54, 1.25	28.16	1.40, 1.11	41.69	2.58
122	119.37	8.00	58.40	4.16	32.54	2.04	25.78	1.64	29.36	1.76	41.69	3.05
188	119.69	9.00	56.01	4.60	33.34	1.84, 2.00	24.98	1.55	29.76	1.74	41.69	3.04

Met, residue no.	N	HN	C^α	H^α	C^ϵ	H^ϵ	Met, residue no.	N	HN	C^α	H^α	C^ϵ	H^ϵ
143	126.89	7.29	53.40	4.96	19.07	2.25	219	?	?	52.70	4.75	?	?

Phe, residue no.	N	HN	C^α	H^α	C^β	H^β	C^δ	H^δ	C^ϵ	H^ϵ	C^ζ	H^ζ
83	?	?	54.06	4.18	38.45	2.35, 1.84	129.51	6.77	131.11	7.41	127.80	7.11
86	118.10	7.58	58.97	4.34	?	?	?	?	?	?	?	?
132	118.46	8.16	55.61	5.66	42.88	2.84	?	?	?	?	?	?
146	120.55	9.58	56.19	5.34	41.69	2.84, 2.70	?	?	?	?	?	?
154	114.20	7.66	57.89	4.29	?	?	?	?	?	?	?	?
157	120.46	8.28	56.86	5.02	38.36	3.10, 3.98	?	?	?	?	?	?
180	122.17	8.89	56.60	4.30	41.50	2.29, 1.92	130.75	6.37	?	?	?	?
196	119.07	8.41	60.38	4.08	37.71	3.45, 3.24	131.04	7.24	128.89	6.61	?	?
232	121.12	7.41	59.59	4.24	39.70	3.18, 2.92	131.22	7.24	?	?	?	?

Pro, residue no.	C^α	H^α	C^β	H^β	C^γ	H^γ	C^δ	H^δ	Pro, residue no.	C^α	H^α	C^β	H^β	C^γ	H^γ	C^δ	H^δ
87	?	?	?	?	?	?	51.11	3.70	170	63.75	3.07	32.91	0.59, −0.03	?	?	49.60	3.63, 2.95
90	62.77	4.37	31.35	1.97, 1.65	?	?	50.84	3.73, 3.64	172	62.37	4.74	33.34	2.36, 2.11	?	?	49.64	3.60
106	62.53	4.65	?	?	?	?	51.24	4.46, 3.66	221	64.76	3.55	30.95	0.71, 1.65	26.78	1.35	50.44	3.33, 2.08
109	61.58	4.55	32.54	2.48, 2.08	24.26[b]	2.14, 2.12	50.44	3.44, 3.90	248	60.78	4.24	30.55	1.85, 2.32	27.60	2.11, 1.94	49.64	3.49
129	61.58	4.96	31.74	2.25, 2.15	?	?	51.24	3.76, 3.26	249	63.57	4.39	31.35	1.91, 2.34	?	?	50.44	3.57, 3.79
156	?	?	?	?	?	?	50.01	3.70, 3.47	250	62.37	4.46	32.14	2.29, 1.95	?	?	50.84	3.85, 3.69
160	63.57	3.97	31.53[b]	2.29, 1.84	?	?	?	?	253	62.77	4.51	32.14	2.30, 2.00	?	?	50.84	3.79

Ser, residue no.	N	HN	C^α	H^α	C^β	H^β	Ser, residue no.	N	HN	C^α	H^α	C^β	H^β
115	112.35	8.05	60.78	4.29	62.77	3.94, 4.03	225	115.61	8.20	57.60	4.12	63.17	3.82
133	117.30	8.72	56.890	4.97	65.16	3.67, 3.91	235	118.12	8.47	57.60	4.58	65.16	4.24, 4.09
145	118.67	8.52	56.41	5.08	65.95	3.77	244	119.37	7.87	61.18	4.26	61.18	4.01
206	119.51	8.45	55.21	4.74	62.37	4.88, 4.24	252	116.41	8.06	55.61	4.80	63.17	3.87, 3.82
212	115.20	7.15	?	?	64.75	4.44, 3.43							

Thr, residue no.	N	HN	C^α	H^α	C^β	H^β	C^γ	H^γ	Thr, residue no.	N	HN	C^α	H^α	C^β	H^β	C^γ	H^γ
85	112.36	8.42	59.99	4.78	69.53	4.99	22.20	1.35	190	109.17	8.14	61.18	4.62	67.54	4.84	22.60	1.29
95	105.36	8.01	60.64	4.34	68.74	4.34	21.80	1.15	191	115.16	8.24	63.53	4.24	69.14	4.24	22.20	1.32
98	111.06	9.29	57.60	5.80	72.32	4.13	22.20	1.18	193	122.91	8.50	61.98	3.78	67.54	2.91	24.98	0.38
105	?	?	55.21	5.01	66.75	3.22	19.81	0.46	215	117.35	8.13	63.57	2.73	67.94	3.86	22.20	1.01
128	110.95	7.65	59.59	5.48	71.52	4.24	24.98	1.55	227	114.31	8.16	63.25	4.19	68.74	4.19	22.20	1.26
131	110.39	8.12	59.19	4.62	71.92	4.10	21.80	1.11	230	111.89	8.45	63.57	4.18	68.34	4.30	22.20	1.33
187	111.23	8.88	59.19	4.95	71.92	4.48	22.00	1.12	255	120.16	7.71	62.37	4.20	69.93	4.26	22.20	1.20

Table I (Continued)

Trp,[f] residue no.	N	HN	C^α	H^α	C^β	H^β	C^δ	H^δ	N^ϵ	$H^{\epsilon 1}$	$C^{\zeta 2}$	$H^{\zeta 2}$	$C^{\eta 2}$	$H^{\eta 2}$	$C^{\zeta 3}$	$H^{\zeta 3}$	$C^{\epsilon 3}$	$H^{\epsilon 3}$
92	123.33	8.22	57.35	4.55	30.36[b]	3.26, 3.55	125.98	7.45	129.76	10.65	112.20	7.54	124.16	7.54	120.84	7.11	120.19	7.83
124	117.55	6.66	57.34	4.75	30.58[b]	3.17, 3.08	128.15	7.36	126.55	9.91	114.40	7.40	122.20	6.87	120.17	6.87	117.72	7.42
186	131.32	9.64	57.16	5.07	30.55	3.13	127.89	7.60	126.26	9.55	115.02	8.18	122.47	7.15	?	?	120.84	7.44

Tyr, residue no.	N	HN	C^α	H^α	C^β	H^β	C^δ	H^δ	C^ϵ	H^ϵ	Tyr, residue no.	N	HN	C^α	H^α	C^β	H^β	C^δ	H^δ	C^ϵ	H^ϵ
99	117.74	8.63	54.90	5.70	42.27	2.70	?	6.74	116.54	6.39	168	118.83	7.83	56.04	4.42	42.84	2.95	133.06	6.90	115.31	6.23
104	111.90	8.02	58.00	4.31	38.11	2.52, 2.86	131.25	7.07	117.27	7.04	220	129.01	7.97	57.55	5.01	39.29	3.92, 3.13	134.06	7.26	117.32	6.83
136	119.38	9.19	58.37	4.44	39.70	3.36, 2.73	131.96	7.22	116.57	6.80	223	125.67	7.98	58.22	2.18	39.78[b]	1.86, 2.03	131.34	6.36	116.53	6.68
155	117.42	6.92	54.09	4.96	39.30	2.09, 2.89	132.62	6.99	116.88	6.83	246	112.59	7.49	58.39	4.82	41.70[b]	3.46, 2.66	133.06	7.34	116.58	6.83

Val, residue no.	N	HN	C^α	H^α	C^β	H^β	C^γ	H^γ	Val, residue no.	N	HN	C^α	H^α	C^β	H^β	C^γ	H^γ
102	130.02	9.55	65.56	3.46	32.94	2.10	21.40, 23.79	1.01, 1.05	127	105.06	7.06	59.59	4.75	32.09	2.70	21.80, 19.41	0.96, 1.18
113	121.47	7.58	65.95	3.57	31.35	2.63	21.80, 24.58	0.98, 0.95	148	112.00	8.20	59.19	5.02	35.82	2.25	23.30, 19.02	0.95, 0.90
117	115.67	8.05	66.34	3.30	31.35	2.08	22.00, 22.60	0.56, 0.76	163	107.33	10.60	66.35	3.90	31.74	2.65	23.39, 23.39	1.34, 1.18
123	114.66	7.53	64.76	3.85	31.35	2.10	22.20, 21.80	0.65, 0.89	198	114.20	7.68	66.35	4.02	32.09	2.47	24.58, 24.58	1.38, 1.49

[a] Resonances assigned by the methods discussed in the text. Residues are numbered according to the sequence of pro-sfSTR; thus the N-terminus is Phe-83 in sfSTR. Residues for which no resonances have been assigned are Gly-88, Gly-159, and Phe-210. [b] The ^{13}C and its one-bond coupled ^1H resonances were assigned by NOE data. [c] Two additional Gln and Asn amide side chain groups that have not been specifically assigned resonate at 7.07 (^1H), 8.41 (^1H), and 109.75 (^{15}N) ppm; and 6.69 (^1H), 7.14 (^1H), and 111.3 (^{15}N) ppm. [d] Two imidazole systems are observed that must belong to His-96 and -224. The resonances are 7.05 ($H^{\delta 2}$), 8.29 ($H^{\epsilon 1}$), 176.56 and 183.28 ($N^{\delta 1}$, $N^{\epsilon 2}$); 7.27 ($H^{\delta 2}$), 8.66 ($H^{\epsilon 1}$), 173.75 and 180.15 ($N^{\delta 1}$, $N^{\epsilon 2}$). [e] These resonances were observed at 20 °C. [f] An additional Trp system consisting of relatively intense resonances was observed in HCCH TOCSY spectra, but not in NOESY spectra. The chemical shifts of this system are 114.95 and 7.54 ppm ($C^\zeta H$), 124.67 and 7.26 ppm ($C^{\eta 2}H$), 122.11 and 7.17 ppm ($C^{\zeta 3}H$), 120.62 and 7.59 ppm ($C^{\epsilon 3}H$). The intensity of the resonances of this system and the absence of NOEs suggest that these resonances belong to a contaminant.

the 14 Pro spin systems, although most have been partly assigned in 3D HCCH COSY and TOCSY spectra and specifically assigned by $H\alpha(i)$–$H\delta(i+1)$ NOEs in 3D ^{13}C NOESY-HMQC spectra. Assignments obtained by these experiments for inhibited sfSTR are in Table I.

Secondary Struture of Stromelysin-1. A summary of the sequential connectivities by both *J* connectivities and NOEs, and NH protons that are exchanging slowly in ^1H–^2H experiments, is described in Figure 4. These data indicate that two helices encompass the regions Asp-111 to Val-127 (structural helix) and Leu-195 to Ser-206 (catalytic helix), a conclusion supported by short-range NOE connectivities (Figure 4) and $^{13}C^\alpha$ and $^{13}C^\beta$ chemical shift patterns (Figure 3). The catalytic helix encompasses the conserved region HEXXH analogous to the catalytic helix of thermolysin (Mathews et al., 1972) and astacin (Bode et al., 1992; Gömis-Ruth et al., 1993). A helical wheel plot of the structural helix shows that it is amphipathic in sfSTR (Figure 5A). Although the topology of the two helices of sfSTR is similar to those in the N-terminal domain of astacin, the amphipathic character of the structural helix is not apparent in the latter protein. A third region of contiguous d_{NN} NOEs spanning residues Asp-238 to Gly-247 suggests the presence of a third helix. Although chemical shift (Figure 3) and NH exchange data (Figure 4) support the presence of this helix, short-range NOEs typical of helix have not been observed, suggesting that this helix is either distorted or mobile. While there are many segments of contiguous $d_{\alpha N}$ NOEs, determination of the presence of β-sheet requires assignment of long-range NOE data. Analysis of the 3D NOESY-HMQC spectra shows a number of NOEs that delineate a four-stranded β-sheet with three parallel strands and one antiparallel strand (Figure 5C). The participation of these residues in β-sheet is futher supported by chemical shift (Figure 3) and NH exchange data (Figure 4). Comparison to astacin shows a similar β-sheet, although for astacin the β-sheet contains four parallel strands and one antiparallel strand (Bode et al., 1992; Gömis-Ruth et al., 1993). A fifth strand analogous to astacin would succeed the first

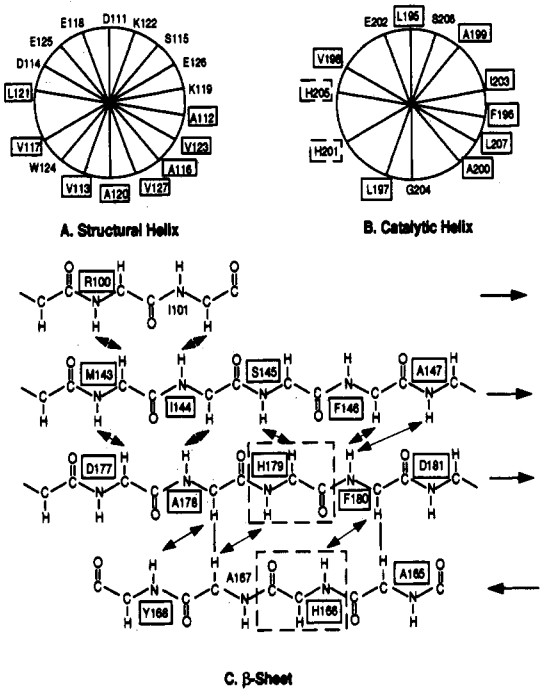

FIGURE 5: Helical wheels are shown for (A) the structural helix spanning Asp-111 to Val-127 and (B) the catalytic helix spanning Leu-195 to Ser-206 of inhibited sfSTR. Hydrophobic residues are boxed. His-201 and -205 are enclosed by dashed lines. (C) The β-sheet of inhibited sfSTR. Double-headed arrows indicate interstrand NOEs. Slowly exchanging NH protons are boxed. The juxtaposition of the His residues 166 and 179 are shown. Residues are numbered according to the sequence of pro-sfSTR.

helix, which spans Asp-111 to Val-127. Indeed, sequential NOE and chemical shift data suggest that the region Thr-131 to Ser-133 does form an extended structure. NH exchange data suggest that these residues form hydrogen bonds (Figure 4); however, the crucial interstrand NOEs have not been observed. Further, the NH protons of Tyr-99, Ile-101, or Asn-103, which would be hydrogen bond donors to a "fifth"

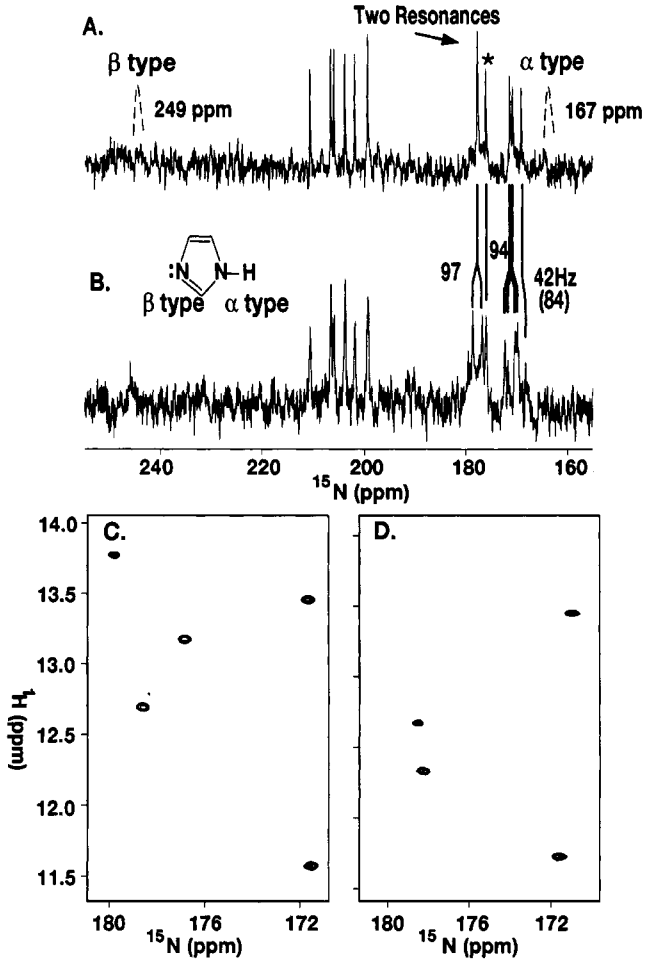

FIGURE 6: Spectra of the imidazole nitrogens of sfSTR and pro-sfSTR. Residues are numbered according to the sequence of pro-sfSTR. (A) Portion of ^{15}N-detected ^{1}H-decoupled spectrum of 1 mM inhibited ^{15}N sfSTR in 50 mM MES, pH 6.5, 5 mM $CaCl_2$, and 0.01% NaN_3 and 37 °C showing the His imidazole nitrogen resonances. (B) Same as (A) except of a ^{15}N-detected and ^{1}H-coupled spectrum. The splitting of three resonances by $^{1}J_{NH}$ (95 Hz) is shown. A fourth resonance appears to broaden and show a coupling of approximately 84 Hz. The resonance marked (*) does not show a coupling. (C) Portion of a 2D ^{1}H, ^{15}N HSQC spectrum of 1 mM [^{15}N]pro-sfSTR in 50 mM acetate-d_3, pH 5.5, 5 mM $CaCl_2$, and 0.01% NaN_3 and 20 °C showing five correlations of His imidazole ^{15}NH, and (D) same as (C) except for inhibited sfSTR where four correlations are observed.

strand, do not appear to be exchanging slowly (Figures 4 and 5), which is consistent with a four-stranded β-sheet.

Characterization of His Imidazole Nitrogens. The ^{1}H-decoupled ^{15}N spectrum of inhibited sfSTR or pro-sfSTR shows the usual peptide NH resonances centered near 120 ppm, the upfield resonances of the Lys and Arg side chain NH moieties, and a cluster of downfield resonances spanning 170–200 ppm that are assigned to His imidazole nitrogens. Expansion of this latter region (Figure 6A) shows two groups, each consisting of six resonances, arising from the imidazole nitrogens, $N^{\delta 1}$ and $N^{\epsilon 2}$, of six His. There are eight His in sfSTR and nine in pro-sfSTR. Within the MMP family only six of these, all in the catalytic domain, are invariant at positions 151, 166, 179, 201, 205, and 211 (Murphy et al., 1991).

An imidazole nitrogen of His can exist in three forms. In model systems a protonated nitrogen (type α) resonates near 167 ppm, a positively charged protonated nitrogen (type α+) near 176 ppm, and a deprotonated nitrogen (type β) near 249 ppm (Bachovchin, 1986) (referenced to liquid NH_3: Srinivasan & Lichter, 1977; Live et al., 1984). The imidazole nitrogens of the upfield group, in the spectra of sfSTR, resonate between 169 and 178 ppm, suggesting that these resonances are either type α or α+. The nitrogens of the downfield group resonate between 199 and 211 ppm. These latter resonances are at least 32 ppm downfield of the expected chemical shift of type α, 23 ppm downfield of type α+, and 38 ppm upfield of type β. Therefore, assignment of the protonation state of the downfield group of nitrogens, on the basis of chemical shift alone, is not possible. Several additional experiments, however, provide evidence that the downfield group of resonances is type β and the upfield group is type α. For instance, the multiplicity of the downfield six resonances does not change in ^{1}H-coupled spectra, compared to ^{1}H-decoupled, whereas the region of the upfield resonances becomes considerably more complicated, with a number of resonances splitting into doublets in the ^{1}H-coupled spectra (Figure 6A,B). Resonances that show proton coupling should be observable in 2D ^{1}H, ^{15}N HSQC experiments (Figure 6C,D). In spectra of pro-sfSTR five correlations are observed, all belonging to the upfield group, whereas in spectra of inhibited sfSTR four correlations are observed to the upfield group. Increasing temperature reduces the number of observed correlations in spectra of inhibited sfSTR to where only two are observed at 40 °C. For the experimental conditions of pH 5.5 and 6.5 and temperatures between 10 and 40 °C no correlations have been observed to the downfield group for either pro-sfSTR or inhibited sfSTR. These data are interpreted as follows. For a correlation to be observed in the HSQC experiment, a proton must spend at least several milliseconds attached to a nitrogen, a time scale set by the coupling constant ($^{1}J_{NH}$ = 95 Hz) and chemical shift difference to water (Jardetsky & Roberts, 1981). The exchange rate constant for free imidazole NH protons is greater than 10^3 min^{-1}, and thus they are not usually observed (Wüthrich, 1986). These observations suggest that there are conditions where at least five imidazole NH protons are not subject to rapid exchange. Further evidence confirming that the imidazole rings of six His are in unusual environments is that the chemical shifts of all resonances in both the upfield and downfield groups are pH independent over the range of 5–7.5 ($\Delta\delta < 0.2$ ppm for the downfield group $\delta\Delta < 0.4$ ppm for the upfield group observed in ^{1}H-decoupled ^{15}N spectra of pro-sfSTR, data not shown). Imidazole nitrogens are typically sensitive to protonation state: a pH titration over the range of 8.0–4.0 leads to an upfield shift of 55 ppm for the deprotonated nitrogen, $N^{\delta 1}$ in free His, and a shift of 5 ppm for the protonated nitrogen, $N^{\epsilon 2}$ in free His (Blomberg et al., 1977). As all resonances in pro-sfSTR remain unaffected within this pH range, the pK_a's must be shifted from the expected pK_a of 6.38 (Tanokura et al., 1976) by at least 1.5 pH units.

Two phenomena that could explain the above spectral properties of the imidazole nitrogens are hydrogen bonding or metal ligation. The resonance of a His imidazole nitrogen shifts approximately 10 ppm upfield if the nitrogen is an acceptor of a proton in a hydrogen bond and 10 ppm downfield if the nitrogen is donating a proton (Bachovchin, 1986). Upfield shifts greater than 10 ppm have been reported for the His $N^{\epsilon 1}$ ligated to the heme iron in cytochrome c_2 labeled with ^{15}N (Yu & Smith, 1988; Gooley & MacKenzie, 1990). Subtracting the ring current effects of the heme moiety (Giessner-Prettre & Pullman, 1971), the ligating nitrogen of the His shifts by approximately 64 ppm upfield in these cytochromes. The upfield group of imidazole nitrogens of sfSTR are 2–11 ppm downfield (Figure 6A) of the expected position of 167 ppm, for a type α nitrogen, indicating that several may be involved in donating protons in hydrogen bonds. The downfield group of imidazole nitrogens are shifted 39–49 ppm upfield

from the expected position of 249 ppm for type β nitrogens, substantially further than the 10 ppm expected for a nitrogen accepting a proton. Therefore, the substantial upfield shift of these latter resonances is ascribed to metal ligation. These shifts, however, are smaller than those observed for the cytochromes, possibly because of differences in ligation and metal ion (Fe^{2+} compared to Zn^{2+}). Another possible explanation is that both the downfield and upfield nitrogens are protonated (type α+) and that the exchange rate of the downfield imidazole NH protons is fast and thus coupling is not observed. In this case, the downfield resonances would have an expected chemical shift of 176 ppm (Bachovchin, 1986). However, hydrogen bonding would not account for the 23–25 ppm downfield shift of the downfield group of resonances from this reference point, concluding that the latter explanation is incompatible with the data.

Assignments of the Zinc His Ligands. The catalytic region HEXXHXXGXXH of astacin is conserved in both the MMP and astacin families (Murphy et al., 1991; Dumermuth et al., 1991; Bode et al., 1992; Gömis-Ruth et al., 1993). Determination of the secondary structure of sfSTR shows, as expected, that two invariant His residues, 201 and 205, are juxtaposed in the catalytic helix (Figure 5), analogous to the conserved HEXXH portion of the catalytic helix of astacin (Bode et al., 1992; Gömis-Ruth et al., 1993) and thermolysin (Mathews et al., 1972). The His residue, 211, analogous to the third His of the catalytic region of astacin, is not located in regular secondary structure. The three His residues, 151, 166, and 179, are invariant in the MMP family, but not in the astacin family (Dumermuth et al., 1991) or thermolysin. The latter two residues are located on opposite strands, but on the same face of the β-sheet (Figure 5). His-151 is not located in a region of regular secondary structure. Thus, delineation of the secondary structure shows that two clusters of His, each consisting of at least two residues, are present.

To further characterize these His clusters, 3D ^{13}C NOESY-HMQC spectra have been analyzed. Before assigning long-range NOEs that involve the His residues, it is necessary to assign the imidazole ring resonances. These assignments were accomplished by a combination of 3D ^{13}C NOESY-HMQC, 2D ^{1}H, ^{15}N HMQC spectra, and selective labeling experiments. Slices from 3D ^{13}C NOESY-HMQC spectra that show NOEs involving the $C^{\delta 2}H$ and $C^{\epsilon 1}H$ protons of a number of His residues are shown in Figure 7. Assignment of the $C^{\delta 2}H$ protons of an aromatic ring is typically based on intraresidue NOEs between these protons and the $C^{\beta}H$ protons where, for steric reasons, the χ_2 rotamers of approximately $\pm 60°$ are generally favored (Ponder & Richards, 1987). These NOEs are clearly observed for His-151 and -179 (Figure 7A). For His residues a χ_2 rotamer of near 180° is also allowed. In the case where χ_1 is 180° or –60° the NOEs between the $C^{\delta 2}H$ and the $C^{\beta}H$ protons are weak or undetectable, but a strong NOE between the $C^{\delta 2}H$ and the $C^{\alpha}H$ is observed. Such an NOE is observed for His-211 (Figure 7B). The assignment of the $C^{\delta 2}H$ protons of His-201 and -205 is ambiguous because both $C^{\delta 2}H$ protons show weak NOEs to a $C^{\beta}H$ of His-205 (Figure 7B). A 2D ^{15}N NOESY HMQC experiment, where the decoupling field strength is sufficient to encompass the imidazole nitrogens, shows a correlation between the NH imidazole at 12.41 ppm and protons at 7.69 and 2.38 ppm (Figure 7C). These NOEs are consistent with the protons assigned to the $N^{\delta 1}H$, $C^{\epsilon 1}H$, and $C^{\beta}H$ of His-201, respectively. As discussed below and shown in Figure 8A, the $C^{\epsilon 1}H$ resonance is correlated with the $C^{\delta 2}H$ at 6.51 ppm, thus assigning this resonance to His-201 and the $C^{\delta 2}H$ at 7.55 ppm to His-205. For reasons that have not been determined,

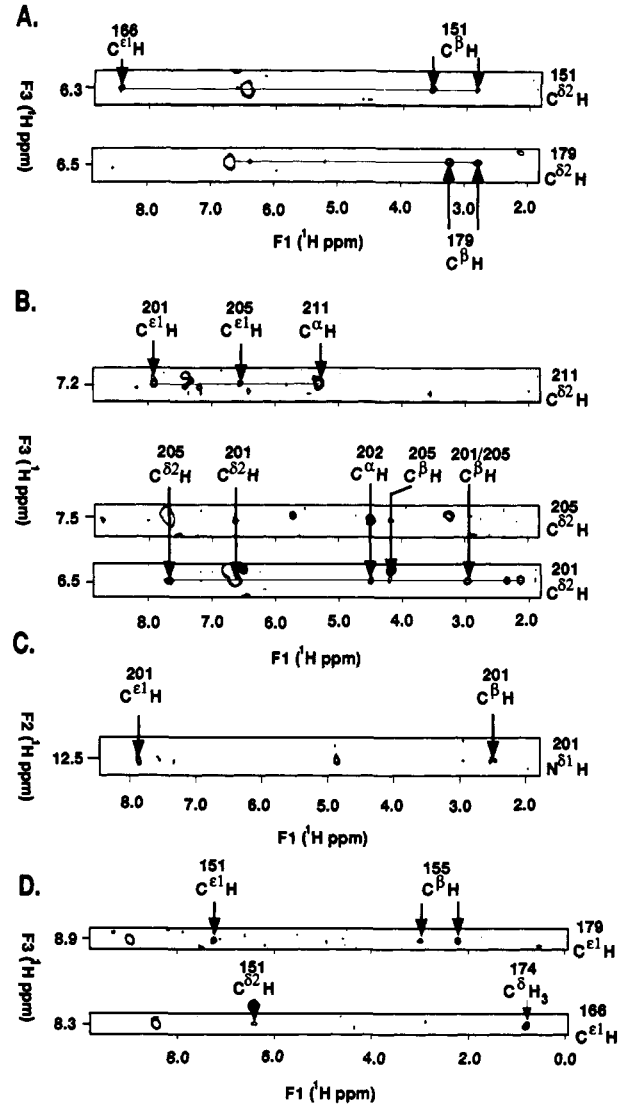

FIGURE 7: Portions of 3D ^{13}C and 2D ^{15}N NOESY-HMQC spectra of sfSTR. Sample conditions were 0.4 mM inhibited ^{15}N, ^{13}C or ^{15}N sfSTR in 50 mM acetate-d_3, pH 5.5, 5 mM $CaCl_2$, and 0.01% NaN_3 and 40 °C. Residues are numbered according to the sequence of pro-sfSTR. (A) Strips from 3D ^{13}C NOESY-HMQC spectra assigning the $C^{\delta 2}H$ of His-151 and -179. The ^{13}C chemical shifts are 125.89 ppm (His-151) and 122.76 ppm (His-179). (B) Strips from 3D ^{13}C NOESY-HMQC spectra assigning the $C^{\delta 2}H$ of His-201, -205, and -211. The ^{13}C chemical shifts are 125.74 ppm (His-201), 126.73 ppm (His-205), and 124.76 ppm (His-211). (C) Portion of a 2D ^{15}N NOESY-HMQC spectrum showing intraresidue NOEs from the $N^{\delta 1}H$ of His-201. (D) Strips from 3D ^{13}C NOESY-HMQC spectra at the $C^{\epsilon 1}H$ resonances of His-179 (139.52 ppm) and His-166 (138.55 ppm).

intraresidue NOEs between the backbone and imidazole resonances of His-166 have not been observed; however, assignments of these resonances are based on NOEs to residues that are proximal to His-166 (see below).

A 2D ^{1}H, ^{15}N HMQC spectrum acquired in ^2H_2O and optimized for two- and three-bond couplings from the $C^{\delta 2}H$ and $C^{\epsilon 1}H$ protons to the imidazole nitrogens extends the assignments to include all resonances except the $^{13}C^{\epsilon}$ (Figure 8A and Table I). The assignment of these latter resonances is based on their unique ^{13}C chemical shifts near 138 ppm. From the HMQC experiment, the protonation state of the individual His residues can be established because the patterns of correlation differ for the $N^{\epsilon 2}H$ and the $N^{\delta 1}H$ tautomers due to coupling and chemical shift differences. Correlations arise from the two-bond couplings $^2J_{N^{\delta 1}H^{\epsilon 1}}$, $^2J_{N^{\epsilon 2}H^{\epsilon 1}}$, and $^2J_{N^{\epsilon 2}H^{\delta 2}}$ and the three-bond coupling $^3J_{N^{\delta 1}H^{\delta 2}}$ (Pelton et al., 1993). For

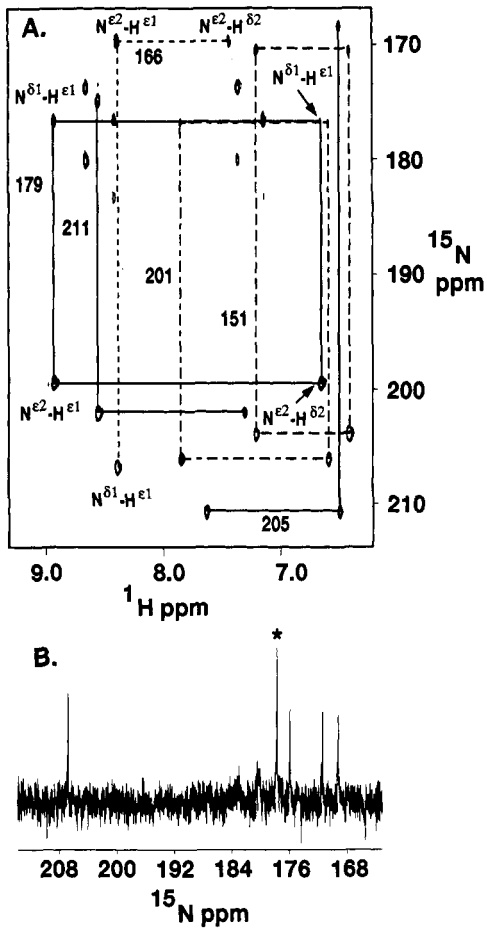

FIGURE 8: Assignment of the imidazole resonances of the His residues in sfSTR. Residues are numbered according to the sequence of pro-sfSTR. (A) Portion of a 2D ^{1}H, ^{15}N HMQC spectrum acquired at 600 MHz on 0.5 mM inhibited ^{15}N sfSTR in 50 mM acetate-d_3, pH 5.5, 5 mM $CaCl_2$, 0.01% NaN_3, and 100% $^{2}H_2O$ and 40 °C. To simplify the figure, only the $N^{\delta 1}$, $N^{\epsilon 2}$, $C^{\delta 2}H$, and $C^{\epsilon 1}H$ correlations for His-166 and -179 are indicated. The pattern of assignment for His-151, -201, -205, and -211 is similar to that of His-179, except for His-205 and -211 the three-bond $N^{\delta 1}H^{\epsilon 1}$ correlation is absent, and for His-205 the $C^{\epsilon 1}H$ is upfield of the $C^{\delta 2}H$ proton. Due to the lack of data, the remaining correlations, which must belong to His-96 and -224, cannot be specifically assigned. (B) A 1D ^{15}N spectrum acquired at 600 MHz of inhibited [$^{15}N^{\delta 1}$]His-labeled sfSTR in 50 mM acetate-d_3, pH 5.5, 5 mM $CaCl_2$, 0.01% NaN_3, and 100% $^{2}H_2O$ and 40 °C. The peak marked (*) is two resonances (compare with Figure 6A).

a His residue, under basic conditions, these couplings are –9.6, –8.8, –6.6, and –2.2 Hz, presumably, for the predominant $N^{\epsilon 2}H$ tautomer (Blomberg et al., 1977). For the $N^{\epsilon 2}H$ tautomer, the $N^{\delta 1}$ resonance will be downfield of the $N^{\epsilon 2}$ resonance, and strong correlations are expected from both the $N^{\epsilon 2}$ and $N^{\delta 1}$ to the $C^{\epsilon 1}H$ proton and a slightly weaker correlation from $N^{\epsilon 2}$ to the $C^{\delta 2}H$ proton. For the $N^{\delta 1}H$ tautomer, the $N^{\delta 1}$ resonance will be upfield of the $N^{\epsilon 2}$ resonance. As the deprotonated nitrogen, compared to the protonated nitrogen, should be coupled more strongly to the imidazole carbon protons, strong correlations are expected from the $N^{\epsilon 2}$ to both the $C^{\epsilon 1}H$ and $C^{\delta 2}H$ protons and weak correlations from $N^{\delta 1}$ to both $C^{\epsilon 1}H$ and $C^{\delta 2}H$ protons. The latter correlation arises from a $^{3}J_{N^{\delta 1}H^{\delta 2}}$ of approximately –3.0 Hz (Blomberg et al., 1977; Pelton et al., 1993). In Figure 8A strong correlations are observed between the $N^{\epsilon 2}$ resonances and both the $C^{\delta 2}H$ and $C^{\epsilon 1}H$ for His-151, -179, -201, -205, and -211, suggesting that the $N^{\epsilon 2}$ is deprotonated for these residues. Strong correlations are observed for the $C^{\epsilon 1}H$ proton to both the $N^{\delta 1}$ and $N^{\epsilon 2}$ resonances for His-166, indicating that the $N^{\delta 1}$ is deprotonated for this residue. To support the conclusion that five His are in the $N^{\delta 1}H$ tautomer and one His is in the $N^{\epsilon 2}H$ tautomer, 1D ^{15}N spectra were acquired on samples of inhibited sfSTR (Figure 8B) and pro-sfSTR selectively labeled with [$^{15}N^{\delta 1}$]His. These spectra show that the $N^{\epsilon 2}$ is deprotonated for five His residues and that the $N^{\delta 1}$ is deprotonated for one His residue.

On the basis of extensive sequential assignments, delineation of the secondary structure, and assignment of the imidazole ring resonances, interresidue NOEs from the imidazole protons consistent with the formation of two clusters of His can be described. The $C^{\delta 2}H$ of His-205 shows an NOE to the $C^{\delta 2}H$ assigned to His-201 (Figure 7B). Both these $C^{\delta 2}H$ show NOEs to a $C^{\beta}H$ of His-205 and the $C^{\alpha}H$ of Glu-202, supporting the assignments and the juxtaposition of His-201 and -205 in the catalytic helix (Figure 5B). The $C^{\delta 2}H$ of His-211 shows NOEs to two $C^{\epsilon 1}H$ protons (Figure 7B) assigned to His-201 and -205 (Figure 8A). The $C^{\epsilon 1}H$ resonance of His-201 shows NOEs to the $C^{\alpha}H$ of Pro-221 (not shown). These data support a model in which the peptide segment 208–212 loops back, positioning His-211 to form the cluster analogous to the three His ligating the single zinc in astacin (Bode et al., 1992). Independent data not involving the His residues that agree with this model include NOEs between Tyr-223 and Val-198 (not shown). Presumably, additional ligands to the catalytic zinc would be the carboxyl oxygens of the inhibitor, although this remains to be demonstrated.

The second zinc site is characterized by the location of His-166 and -179 on opposite strands, but on the same face of the β-sheet, and by a number of long-range NOEs from two His $C^{\epsilon 1}H$ protons (Figure 7D). The $C^{\epsilon 1}H$ of His-179 shows NOEs to both the $C^{\epsilon 1}H$ of His-151 and the $C^{\beta}H$ protons of Tyr-155, clearly indicating that His-151 and -179 are proximal to each other. The $C^{\epsilon 1}H$, tentatively assigned to His-166, shows NOEs to both the $C^{\delta 2}H$ of His-151 and the $C^{\delta}H_3$ of Ile-174, suggesting that this residue is also near His-151. At this point, additional ligands have not been identified for this second zinc; however, NOEs between the $N^{\delta 1}H$ of His-151 to the peptide NH of Phe-157 and from the $C^{\alpha}H$ of Asp-181 to the $C^{\delta 2}H$ of His-151 and -166 suggest that the invariant residues Asp-158 and -181, respectively, are near this site. Other invariant residues that are potential ligands and that are within this region include Asp-153 and Glu-184. NOEs have not been observed between residues near His-151, -166, and -179 to residues near His-201, -205, and -211, suggesting that the two clusters are separate and independent, agreeing with EXAFS data (Holz et al., 1992). The final proof of these observations will be the calculation of structures, which is presently occurring in our laboratories.

These experiments have established not only the specific His residues ligating the metal ions, but also which tautomer is involved in the ligation. The three His residues, 201, 205, and 211, that ligate the catalytic zinc are all in the $N^{\delta 1}H$ tautomer. This pattern is identical to the ligation of the catalytic zinc astacin, and thus, within this region, both the primary sequence and the tertiary structure are conserved between astacin and sfSTR. The second zinc site is ligated by two His residues, 151 and 179, that are in the $N^{\delta 1}H$ tautomer, whereas the third His, 166, is in the $N^{\epsilon 1}H$ tautomer. His-166 and His-179 are located on opposite strands of antiparallel β-sheet, and His-151 is in a loop between strands of this sheet (Figure 5). The assignments show that the four imidazole NH correlations observed for sfSTR in ^{1}H, ^{15}N HSQC experiments (Figure 6D) are assigned to His-151, -166, -179, and -201 (Table I). As these correlations are observable, the imidazole NH protons of the three His that ligate the structural zinc and one that ligates the catalytic zinc may be

stabilized by hydrogen bonding, which in turn, may stabilize the zinc by charge distribution. The ligation pattern of the structural zinc appears unique compared to zinc enzymes that have had structures determined (Vallee & Auld, 1990). Zinc ligation by His in antiparallel β-sheet is observed for carbonic anhydrase where the zinc is ligated by two His (located on one strand of antiparallel β-sheet) in the $N^{\delta 1}H$ tautomer, and a third His (located on an opposing strand) in the $N^{\epsilon 2}H$ tautomer (Liljas et al., 1972). Thus, His residues which are on opposing strands of antiparallel β-sheet may find it energetically favorable to adopt different tautomer states in order to ligate metal ions.

CONCLUSION

The chemical shifts and other NMR spectral properties of the imidazole ^{15}N resonances of six His residues suggest that all six are ligated to metal ions, probably the two zincs that have been characterized for sfSTR (Salowe et al., 1992). These data are in agreement with EXAFS results that suggest four nitrogen or oxygen ligands for each zinc (Holz et al., 1992). Assignments of resonances, delineation of the secondary structure of sfSTR, and analysis of long-range NOE data indicate that these His residues form two clusters, each consisting of three residues that are strictly conserved in the MMP family: 201, 205, and 211 in the catalytic site and 151, 166, and 179 in the second site. Five residues (151, 179, 201, 205, 211) are in the $N^{\delta 1}H$ tautomer, and one residue (166) is in the $N^{\epsilon 2}H$ tautomer. Given these conclusions and the sequence homology of other members of the MMP family, we suggest, as a means of assessing the presence and number of His ligands in these proteins, labeling these proteins with ^{15}N and acquiring various direct and indirect ^{15}N spectra. The characteristic chemical shifts of an imidazole nitrogen ligated to metal will indicate the number of metals present. In conclusion, the data presented here show that although sfSTR, a representative member of the MMP family, has a similar topology to astacin, the ligation of two zincs by His residues in sfSTR indicates that there are significant differences, suggesting that the MMP family is a distinct class of metalloendoproteases.

ADDED IN PROOF

The NH resonances of Arg-100 and Ser-133 were missassigned, thus leading to incorrect assignment of Tyr-99, Thr-98, and Leu-97 and Phe-132, Thr-131, and Leu-130. Reanalysis of the NOE data of these residues shows that the β-sheet described in Figure 5 is five stranded, where strand I spans residues Thr-95 to Ile-101; strand II, Leu-130 to Leu-135 (previously not observed); strand III, Ile-142 to Ala-147; strand IV, Ala-165 to Tyr-168; and strand V, Asp-177 to Asp-181. The assignments in Table I have been corrected. We thank Dr. Erik Zuiderweg for communicating the secondary structure observed by his group of the catalytic domain of stromelysin-1 prior to publication.

ACKNOWLEDGMENT

We wish to thank Ms. Catherine K. Smith for preparation of several ^{15}N-labeled samples and Dr. Bruce L. Bush for helpful discussions.

REFERENCES

Bachovchin, W. W. (1986) *Biochemistry 25*, 7751–7759.

Barkhuijsen, H., De Beer, R., Bovee, W. M. M. J., & Van Ormondt, D. (1985) *J. Magn. Reson. 61*, 465–481.

Bax, A., & Subramanian, S. (1986) *J. Magn. Reson. 67*, 565–569.

Bax, A., Clore, G. M., Driscoll, P. C., & Gronenborn, A. G. (1990a) *J. Magn. Reson. 87*, 620–627.

Bax, A., Clore, G. M., & Gronenborn, A. G. (1990b) *J. Magn. Reson. 88*, 425–431.

Bax, A., Ikura, I., Kay, L. E., Torchia, D. A., & Tschudin, R. (1990c) *J. Magn. Reson. 86*, 304–318.

Blomberg, F., Maurer, W., & Ruterjans, H. (1977) *J. Am. Chem. Soc. 99*, 8149–8159.

Bode, W., Gomis-Rüth, F. X., Huber, R., Zwilling, R., & Stöcker, W. (1992) *Nature 358*, 164–167.

Bodenhausen, G., & Ruben, D. J. (1980) *Chem. Phys. Lett. 69*, 185–189.

Boucher, W., Laue, E. D., Campbell-Burk, S. L., & Domaille, P. J. (1992a) *J. Am. Chem. Soc. 114*, 2262–2264.

Boucher, W., Laue, E. D., Campbell-Burk, S. L., & Domaille, P. J. (1992b) *J. Biomol. NMR 2*, 631–637.

Campbell-Burk, S. L., Domaille, P. J., Starovasnik, M. A., Boucher, W., & Laue, E. D. (1992) *J. Biomol. NMR 2*, 639–646.

Dumermuth, E., Sterchi, E. E., Jiang, W., Wolz, R. L., Bond, J. S., Flannery, A. V., & Beynon, R. J. (1991) *J. Biol. Chem. 266*, 21381–21385.

Giessner-Prettre, C., & Pullman, B. (1971) *J. Theor. Biol. 31*, 287–294.

Gomis-Rüth, F. X., Stöcker, W., Huber, R., Zwilling, R., & Bode, W. (1993) *J. Mol. Biol. 229*, 945–968.

Gooley, P. R., & MacKenzie, N. E. (1990) *FEBS Lett. 260*, 225–228.

Holz, R. C., Salowe, S. P., Smith, C. K., Cuca, G. C., & Que, L., Jr. (1992) *J. Am. Chem. Soc. 114*, 9611–9614.

Ikura, M., Kay, L. E., Tschudin, R., & Bax, A. (1990) *J. Magn. Reson. 86*, 204–209.

Jardetsky, O., & Roberts, G. C. K. (1981) *NMR in Molecular Biology*, Academic Press, Inc., London.

Johnson, B. A. (1992) *J. Magn. Reson. 100*, 189–194.

Kay, L. E., Ikura, M., & Bax, A. (1991) *J. Magn. Reson. 91*, 84–92.

LeMaster, D. M., & Richards, F. M. (1985) *Biochemistry 24*, 7263–7268.

Liljas, A., Kannan, K. K., Bergstén, P. C., Waara, I., Fridborg, B., Strandberg, B., Carlbom, U., Järup, L., Lövgren, S., & Petef, M. (1972) *Nature, New Biol. 235*, 131–137.

Live, D. H., Davis, D. G., Agosta, W. C., & Cowburn, D. (1984) *J. Am. Chem. Soc. 106*, 1939–1941.

MacNaul, K. L., Chartrain, N., Lark, M., Tocci, M. J., & Hutchinson, N. I. (1990) *J. Biol. Chem. 265*, 17238–17245.

Maniatis, T., Fritsch, E. F., & Sambrook, J. (1982) *Molecular Cloning—A Laboratory Manual*, Cold Spring Harbor Laboratory, Cold Spring Harbor, NY.

Marcy, A. I., Eiberger, L. L., Harrison, R., Chan, H. K., Hutchinson, N. I., Hagmann, W. K., Cameron, P. M., Boulton, D. A., & Hermes, J. D. (1991) *Biochemistry 30*, 6476–6483.

Mathews, B. W., Jansonius, J. N., Colman, P. M., Schoenborn, B. P., & Dupourque, D. (1972) *Nature, New Biol. 238*, 37–41.

Messerle, B. A., Wider, G., Otting, G., Weber, C., & Wüthrich, K. (1989) *J. Magn. Reson. 85*, 608–613.

Murphy, G. J. P., Hembry, R. M. & Reynolds, J. J. (1986) *Collagen Relat. Res. 6*, 351–363.

Murphy, G. J. P., Murphy, G., & Reynolds, J. J. (1991) *FEBS Lett. 289*, 4–7.

Norwood, T. J., Boyd, J., Heritage, J. E., Soffe, N., & Campbell, I. D. (1990) *J. Magn. Reson. 87*, 488–501.

Pelton, J. G., Torchia, D. A., Meadow, N. D., & Roseman, S. (1993) *Protein Sci. 2*, 543–558.

Ponder, J. W., & Richards, F. M. (1987) *J. Mol. Biol. 73*, 775–791.

Powers, R., Gronenborn, A. M., Clore, G. M., & Bax, A. (1991) *J. Magn. Reson. 94*, 209–213.

Richarz, R., & Wüthrich, K. (1978) *Biopolymers 17*, 2133–2141.

Salowe, S. P., Marcy, A. I., Guca, G. C., Smith, C. K., Kopka, I. E., Hagmann, W. K., Hermes, J. D. (1992) *Biochemistry 31*, 4535–4540.
Saus, J., Quinones, S., Otani, Y., Nagase, H., Harris, E. D., & Kurkinen, M. (1988) *J. Biol. Chem. 263*, 6742–6745.
Spera, S., & Bax, A. (1991) *J. Am. Chem. Soc. 113*, 5490–5492.
Summers, M. F., Marzilli, L. G., & Bax, A. (1986) *J. Am. Chem. Soc. 108*, 4285–4294.
Srinivasan, P. R., & Lichter, R. L. (1977) *J. Magn. Reson. 28*, 227–234.
Tanokura, M., Tasumi, M., & Miyazuwa, T. (1976) *Biopolymers 15*, 393–401.
Vallee, B. L., & Auld, D. S. (1990) *Biochemistry 29*, 5647–5659.
Woessner, J. F. (1991) *FASEB J. 5*, 2145–2154.
Wüthrich, K. (1986) *NMR of Proteins and Nucleic Acids*, John Wiley and Sons, New York.
Yu, L. P., & Smith, G. M. (1988) *Biochemistry 27*, 1949–1956.
Zuiderweg, E. R. P., & Fesik, S. (1989) *Biochemistry 28*, 2387–2391.